Bioprinting 51 (2025) e00439

Contents lists available at ScienceDirect

Bioprinting

journal homepage: www.sciencedirect.com/journal/bioprinting

Research paper

Development of starch-based support material alternately extruded with gelatin-based bioinks for 3D bioprinting application

Pekik Wiji Prasetyaningrum, Wildan Mubarok, Takashi Kotani, Shinji Sakai *

Division of Chemical Engineering, Department of Materials Engineering Science, Graduate School of Engineering Science, The University of Osaka, 1-3 Machikaneyama-cho, Toyonaka, Osaka, 560-8531, Japan

ARTICLE INFO

Keywords:
3D bioprinting
Starch
Gelatin
Horseradish peroxidase
Stem cells

ABSTRACT

The use of support materials is crucial for the 3D bioprinting of low-viscosity bioinks, which yield soft hydrogel constructs susceptible to deformation under their weight. In this study, we developed a starch-based support material that provides structural support during printing and supplies hydrogen peroxide (H_2O_2), for printing cell-laden constructs from low-viscosity bioinks (4.4–53.1 mPa s at 1 s^{-1} shear rate) composed of a gelatin derivative possessing phenolic hydroxyl moieties (gelatin-Ph), horseradish peroxidase (HRP), and cells. Importantly, the support material can be selectively and gently removed using α-amylase, a biocompatible enzyme, without harming the construct or encapsulated cells, which is a significant advancement over conventional methods of removing support systems. 3D constructs were fabricated by alternately extruding bioinks containing 5.0 w/v% gelatin-Ph and 10 U/mL HRP with a support material consisting of 16.7 w/w% starch and 10 mM H_2O_2. Immortalized human bone marrow-derived mesenchymal stem cells encapsulated within the constructs showed >80 % viability after printing and exhibited an elongated morphology and proliferation, while maintaining their stemness over 14 days of culture. The cells underwent osteogenic differentiation when cultured in a differentiation medium, as evidenced by the calcium deposition, alkaline phosphatase activity, and expression of osteogenic genes, demonstrating the potential of the proposed approach for tissue-engineering applications.

1. Introduction

Recently, three-dimensional (3D) bioprinting has emerged as a promising technology for fabricating cell-laden constructs for biomedical applications [1]. Among bioprinting methods, extrusion-based bioprinting is the most widely used because of its simple printing process, compatibility with high-cell-density bioinks, and ability to print inks with a wide viscosity range [2,3]. This versatility is particularly important because the viscosity of the bioink directly influences the mechanical properties of the resulting hydrogel constructs [4,5]. Low-viscosity bioinks, which result in soft hydrogels, have the advantage of reducing the shear stress during extrusion, thereby alleviating cell damage [4–7]. However, printing tall or complex structures with low-viscosity bioinks remains challenging because the structural integrity of these constructs is often compromised owing to their insufficient mechanical strength.

The use of support materials, as in the case of the freeform reversible embedding of suspended hydrogels (FRESH) method, has gained increasing attention for addressing the issues of low-viscosity bioink printing [8–15]. However, a key limitation of this method is the distortion of previously printed portions of the construct due to the displacement of the support material by the newly extruded bioink, which is often mitigated by using a large volume of the support material relative to the bioink [16]. Kotani et al. reported a method in which a high-viscosity support material and low-viscosity bioink were alternately extruded to reduce the use of support materials [17]. Bioinks containing phenol-modified hyaluronic acid and horseradish peroxidase (HRP) were alternately extruded using an H_2O_2-loaded ultrasound gel. This approach enabled the fabrication of soft hydrogels by preventing the construct from deforming post extrusion, while allowing bioink gelation through crosslinking agents diffused from the support material [17]. Despite these promising results, the tunability of the viscosity of ultrasound gels is limited, especially when higher viscosities are required, which restricts the applicability of the gels in printing large and complex structures. Moreover, mechanical extraction or chemical treatment is required to remove the gels, which can compromise the

* Corresponding author.
E-mail addresses: pekikwiji@cheng.es.osaka-u.ac.jp (P.W. Prasetyaningrum), wildanmubarok@cheng.es.osaka-u.ac.jp (W. Mubarok), t.kotani@cheng.es.osaka-u.ac.jp (T. Kotani), sakai@cheng.es.osaka-u.ac.jp (S. Sakai).

https://doi.org/10.1016/j.bprint.2025.e00439
Received 16 May 2025; Received in revised form 19 August 2025; Accepted 12 September 2025
Available online 15 September 2025

integrity of the printed construct and affect the viability of embedded cells. To overcome these limitations, we investigated the use of starch as an alternative.

A starch slurry exhibits pseudoplastic behavior [18], allowing shear-thinning flow, which is ideal for extrusion-based printing. Starch has been incorporated into bioinks to enhance printability and cytocompatibility [19,20]. Recently, Li et al. introduced a removal-free multicellular suspension bath-based 3D bioprinting (SUB3BP) technique using a starch/gelatin hybrid hydrogel [20]. However, the support material permanently remained within the construct, limiting its suitability for applications that require scaffold removal, implantation, or the creation of perfusable structures with minimal residual matrix.

Another key advantage of starch is its enzymatic degradability by α-amylase, which enables the controlled and cytocompatible removal of the support materials. Conventional removal techniques often cause structural damage and reduce the cell viability [21,22]. By contrast, enzymatic degradation offers high specificity, a controlled degradation rate, and mild reaction conditions, minimizing damage to the constructs and embedded cells [23]. α-Amylase is naturally present in humans, confirming its biocompatibility [24]. These properties make starch a promising candidate as a component of support materials.

To the best of our knowledge, no previous study has investigated the use of starch as a multifunctional sacrificial support material that simultaneously provides mechanical support, facilitates the crosslinking of low-viscosity bioinks, and can be removed under mild enzyme-mediated conditions. This novel approach can address the key challenges in printing soft constructs while maintaining cell viability and structural integrity. Therefore, in this study, we aim to evaluate the feasibility of using starch as a sacrificial support material for the 3D bioprinting of bioinks based on low-viscosity gelatin derivatives possessing phenolic hydroxyl moieties (gelatin-Ph). An aqueous solution of gelatin-Ph was gelled via HRP-mediated crosslinking of the phenolic groups [25–27]. Gelatin-Ph has been used as a component of bioinks [28–31]. Recent studies have reported its utilization as a composite bioink component combined with other high-viscosity materials, such as phenol-grafted hyaluronic acid and alginate [32,33]. However, the application of gelatin-Ph as a standalone low-viscosity bioink remains unexplored.

Herein, we present a method for fabricating bioprinted constructs by alternately extruding starch-based support materials containing H_2O_2 with bioinks containing gelatin-Ph, HRP, and immortalized human bone marrow-derived mesenchymal stem cells (UE7T-13) (Fig. 1). After printing, the starch support material was selectively and gently removed through enzymatic degradation using α-amylase. We assessed printability by varying the composition of the support material and inks and evaluated the viability, morphology, and mitochondrial activity of the enclosed cells. Additionally, we investigated the stemness and osteogenic differentiation of cells enclosed within the construct.

2. Materials and methods

2.1. Materials

Type-B bovine gelatin (~225 g bloom) was purchased from Sigma-Aldrich (St. Louis, MO, USA). Starch from wheat, horseradish peroxidase (HRP; 140 and 200 U/mg), H_2O_2 aqueous solution (30 w/w%), *N*-hydroxysuccinimide (NHS), 4-morpholinoethanesulfonic acid (MES), catalase from bovine liver (8000 U/mg), collagenase (190 U/mg), disodium *p*-nitrophenyl phosphate (*p*NPP), alizarin red, and 4 % paraformaldehyde were obtained from FUJIFILM Wako Pure Chemical (Osaka, Japan). 1-Ethyl-3-(3-dimethylaminopropyl) carbodiimide (EDC), α-amylase, and tyramine hydrochloride were purchased from the Peptide Institute (Osaka, Japan), Kishida Chemical (Tokyo, Japan), and Chem-Impex (Wood Dale, IL, USA). Dulbecco's modified Eagle's medium (DMEM) was purchased from Nissui Pharmaceutical (Tokyo, Japan). The osteogenic differentiation kit was purchased from Lonza (Walkersville, MD, USA). Calcein-AM and Triton X-100 were purchased from Nacalai Tesque (Kyoto, Japan). Propidium iodide (PI) and a reagent for cell counting based on mitochondrial activity (Cell Counting Kit-8) were obtained from Dojindo (Kumamoto, Japan). Reagent for RNA isolation (RNA isolation kit) and cDNA synthesis (PrimerScript RT Master Mix) were purchased from Takara Bio (Shiga, Japan).

2.2. Preparation of phenol-grafted gelatin (Gelatin-Ph)

Gelatin-Ph was synthesized as described in Ref. [25]. Briefly, tyramine hydrochloride was conjugated to type-B gelatin by NHS/EDC chemistry in MES buffer (pH 6.0) at 60 °C for 24 h. The product was dialyzed against distilled water in a dialysis tube with a molecular weight cutoff (MWCO) of 12–14 kDa for three days and then freeze-dried. Conjugation of the phenol (Ph) groups was confirmed by ^{1}H NMR (JNM ECS-400; JEOL, Tokyo, Japan) spectroscopy and UV–vis

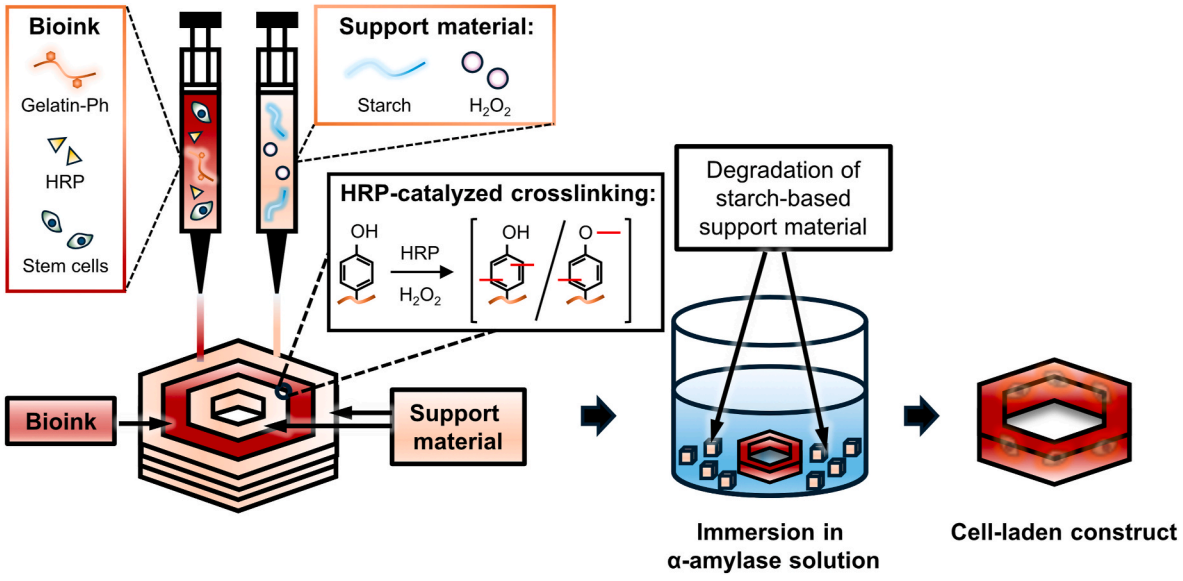

Fig. 1. Schematic illustration of the fabrication of cell-laden construct by alternate extrusion of the support material containing starch and H_2O_2, which induces gelation of the bioinks composed of gelatin-Ph, HRP, and stem cells. Cell-laden construct was collected by degrading the starch using α-amylase.

spectrometry (UV-2600; Shimadzu, Kyoto, Japan) (Fig. S1). The content of Ph groups in gelatin-Ph was determined as 4.05×10^{-4} mol-Ph/g--gelatin-Ph from the UV–vis absorbance at 275 nm using a tyramine standard curve.

2.3. Preparation of support material and ink

Starch (4.8, 9.1, 16.7, and 28.6 w/w%) was suspended in calcium-magnesium-free phosphate-buffered saline solution (PBS; pH 7.4). The H_2O_2 solution was then added to the starch suspension to obtain a final concentration of 1–50 mM H_2O_2. The starch suspension was heated at 80 °C for 5 min, then cooled to room temperature (25 °C) over the course of 1–2 h, resulting in the formation of a starch slurry. This starch slurry was used as the support material for the subsequent experiments.

The inks were prepared by dissolving gelatin-Ph (1.0, 2.5, and 5.0 w/v%) in PBS, followed by the addition of HRP to achieve final concentrations of 1, 5, and 10 U/mL.

2.4. Rheological properties of support material and ink

The viscoelastic properties of the support material and ink were evaluated using a rheometer (HAAKE MARS III; Thermo Fisher Scientific, Waltham, MA, USA) equipped with parallel plates 40 mm in diameter. A 0.65 mL sample was placed in between a 0.5 mm gap, and the viscosity was measured at a shear rate of 0.001–1000 s^{-1}. For the starch slurry prepared using 16.7 w/w% starch, the viscosity was also measured at a shear rate of 1000–0.001 s^{-1}. All measurements were conducted at 25 °C.

2.5. Cell culture

Immortalized human bone marrow-derived mesenchymal stem cells (UE7T-13) obtained from Riken Cell Bank (Ibaraki, Japan) were cultured in DMEM supplemented with 10 v/v% fetal bovine serum (FBS) in a humidified incubator (37 °C, 5% CO_2).

2.6. Extrusion-based bioprinting

2.6.1. Evaluation of printability

Extrusion-based 3D printing was performed using a 3D printer (BIO X, Cellink, Gothenburg, Sweden) equipped with two extruders, each comprising a syringe pump, 2.5 mL syringe, and 25-gauge tapered needle (outer diameter: 0.51 mm, inner diameter: 0.26 mm). The printability was assessed by fabricating hexagonal constructs (ink thickness: 2 mm, support material thickness: 2 mm, height: 2.5 mm, 8 layers) using support materials containing 4.8–28.6 w/w% starch and 1–50 mM H_2O_2, along with inks composed of 1.0–5.0 w/v% gelatin-Ph and 1–10 U/mL HRP. Constructs printed without the support material or using the support material without H_2O_2 were used as controls. To evaluate the feasibility of printing complex constructs, a human nose model (width: 18 mm, length: 24 mm, height: 11 mm, 40 layers) was fabricated using the ink containing 5.0 w/v% gelatin-Ph and 10 U/mL HRP, along with the support material containing 16.7 w/w% starch and 10 mM H_2O_2. The extrusion rate was set to 1.5–3.0 μL/s for the ink and 1.5–2.0 μL/s for the support materials, with a movement speed of 10–15 mm/s. Printing was performed at room temperature (25 °C). After printing, the support materials were removed by soaking the constructs in PBS containing 0.1 w/v% α-amylase for 15–60 min. The average thickness, height, and corner angle of the printed constructs were measured using an image analysis software (ImageJ, 1.64k; NIH, Bethesda, MD, USA) to evaluate the printability.

2.6.2. FRESH printing

FRESH printing, including the preparation of the gelatin slurry bath, was performed under previously reported printing conditions, yielding good results [14]. Briefly, 5.0 w/v% gelatin-Ph supplemented with 10 U/mL HRP ink was extruded into a gelatin slurry bath containing 10 mM H_2O_2. The major particle size of the gelatin slurry ranges from 30 to 150 μm (Fig. S2). Hexagonal shapes were printed with a 25-gauge nozzle using an extrusion rate of 1.8 μL/s and a movement speed of 13 mm/s. After printing, the gelatin bath was removed by heating to 37 °C.

2.6.3. Evaluation of stability of the printed construct

The post-printing stability was assessed using a square construct (length: 11 mm, ink thickness: 1 mm, height: 2.5 mm, 8 layers) printed with ink containing 5.0 w/v% gelatin-Ph and 10 U/mL HRP, along with a support material composed of 16.7 w/w% starch and 10 mM H_2O_2. The stability was determined as the thickness and height ratio of the constructs following immersion in PBS at 37 °C for 14 days relative to that at day 0.

2.6.4. 3D bioprinting

Cell-laden constructs (ink thickness: 1 mm, length: 10 mm, height: 1 mm, 4 layers) were printed by alternately extruding the support material composed of 16.7 w/w% starch and 10 mM H_2O_2 with the bioink containing 5.0 w/v% gelatin-Ph, 10 U/mL HRP, and 1.0×10^6 cells/mL UE7T-13 cells. After printing, the constructs were immersed in the culture medium containing 0.1 w/v% α-amylase and 0.1 w/v% catalase for 1 h to degrade the starch and remaining H_2O_2. The medium was then replaced with growth medium.

2.7. Live/dead staining

Live/dead staining was performed on days 1, 7, and 14 of culture using calcein-AM (live cells) and PI (dead cells). Briefly, the cell-laden constructs were incubated in PBS containing 3.33 μg/mL calcein-AM and 6.67 μg/mL PI for 30 min at 37 °C. After rinsing with PBS, the cells were observed under a fluorescence microscope (BZ-X810; Keyence, Osaka, Japan) and confocal laser-scanning microscope (C2; Nikon, Tokyo, Japan).

2.8. Mitochondrial activity

The mitochondrial activity of the cells in the printed construct was assessed from days 1–14 of culture using a cell counting reagent. Briefly, the cell-laden constructs were incubated in the culture medium containing the reagent at 10 v/v% for 6 h at 37 °C. The mitochondrial activity, reflecting the viable cells within each construct, was quantified by measuring the absorbance at 450 nm using a spectrometer (SpectraMax iD3; Molecular Devices, San Jose, CA, USA).

2.9. Flow cytometry

Flow cytometry was used to evaluate the stemness of the embedded UE7T-13 cells after 14 days of culture based on the expression of CD44, a positive marker, and CD45, a negative marker [34]. The cells were collected by degrading the construct using 0.1 w/v% collagenase in PBS for 30 min and then treated with 0.1 w/v% trypsin solution for 2 min to dissociate the cell aggregates. Cells cultured in a 2D well-plate served as controls. The cells were stained with PBS containing 3.33 μg/mL calcein-AM for 15 min, followed by incubation in a solution containing 50 μg/mL Human BD Fc Block™ for 10 min at room temperature. Finally, the cells were stained with Alexa Fluor 647-conjugated anti-human CD45 and APC-conjugated anti-mouse CD44 (1:300 in PBS) for 30 min at 4 °C. Flow cytometry was conducted using a BD Accuri flow cytometer (BD Biosciences, Franklin Lakes, NJ, USA).

2.10. Osteogenic differentiation

Osteogenic differentiation was induced by replacing the growth medium with osteogenic differentiation medium on day 14 post printing. Differentiation was performed for 26 days.

2.11. Alizarin red staining

Alizarin red staining was performed on days 12 and 26 after cell differentiation. Briefly, the cell-laden constructs were fixed by soaking in 4% paraformaldehyde for 30 min, followed by immersion in alizarin red solution for 60 min. Next, the stained constructs were extensively washed with distilled water until the solution became clear, followed by overnight soaking in distilled water to remove residual alizarin red. The stained calcium deposits were observed under a microscope (BZ-X810; Keyence).

2.12. Alkaline phosphatase (ALP) activity

The ALP activity was measured on days 12 and 26 of cell differentiation. The cells were lysed with 0.1 v/v% Triton X-100 in 50 mM 2-amino-2-methyl-1-propanol (AMP) buffer at 4 °C, and the lysates were collected by centrifugation (12,000×*g*, 10 min, 4 °C). The precipitated lysates were incubated with 5 mM *p*NPP in AMP buffer for 2 h at 37 °C, and the reaction was terminated using 0.1 M NaOH solution. The resulting concentration of *p*-nitrophenolate (*p*NP) was determined from the absorbance at 405 nm using a spectrometer (SpectraMax iD3; Molecular Devices).

2.13. Real-time quantitative polymerase chain reaction (RT-qPCR)

RNA was extracted from the printed and 2D-cultured cells using an RNA isolation kit, followed by reverse transcription using the PrimeScript RT Master Mix reagent kit, according to the manufacturer's instructions. The primer sequences used in this study are listed in Table S1. The expression levels of endoglin (CD105), Sox2, Runx2, Osteocalcin, Col1a1, and GAPDH were quantified using a TB Green Master Kit (Takara Bio). The expression levels of CD105 and Sox2 were quantified using the ΔCT method, where the Ct values were normalized to that of the housekeeping gene GAPDH. The expression levels of Runx2, Osteocalcin, and Col1a1 were calculated using the –ΔΔCT method by applying the following formula:

$$-\Delta\Delta CT = 2^{-\left(\Delta CT_{diff} - \Delta CT_{und}\right)}$$

ΔCT_{Diff} and ΔCT_{Und} refer to the gene expression normalized to that of GAPDH in differentiated and undifferentiated cells, respectively.

2.14. Statistical analysis

The data were analyzed using a spreadsheet software (Excel 2024, Microsoft, Redmond, WA, USA). All data are presented as means ± SD. Statistical analysis was conducted using one-way analysis of variance (ANOVA), followed by a *t*-test using Tukey's honest significant difference (HSD) method. Data were considered significantly different at $p < 0.05$.

3. Results and discussion

3.1. Characterization and printability of support material and ink

3D printing material must meet fundamental criteria, including having optimal rheological properties, such as an appropriate viscosity and shear-thinning behavior, to allow smooth extrusion and to maintain the structural integrity. To meet these criteria, we first examined the gelatinization of starch suspensions at various temperatures (60, 80, and 100 °C) and heating durations (1, 5, and 10 min). Increasing the temperature resulted in a higher viscosity (Fig. S3a). The printing test demonstrated that the starch slurry prepared by heating at 80 °C showed good printability, whereas the slurry prepared by heating at 60 °C was too weak owing to inadequate gelatinization, and that prepared by heating at 100 °C was not extrudable owing to excessive gelatinization (Fig. S3b and c). At a fixed temperature of 80 °C, heating for 5 min resulted in adequate gelatinization, allowing good printability (Fig. S4). In the presence of water, heating causes starch granules to absorb water, swell, and lose their crystalline structure. As heating continues, amylose and amylopectin leach out and the granules eventually rupture [35,36]. High temperatures and prolonged heating cause starch molecules to form a more interconnected gel network that traps water more tightly [37], eventually resulting in the formation of a dry, rigid paste with diminished extrudability, which ultimately compromises the printability of the starch slurry. Based on these results, heating at 80 °C for 5 min was selected as the condition for preparing the starch-based support material.

Next, we evaluated the effect of the starch concentration on the rheological properties of the support material. A concentration-dependent increase in the viscosity was observed, where the highest viscosity was observed with 16.7 w/w% starch (Fig. 2a). The starch slurry also exhibited shear-thinning behavior (Fig. 2a), as evidenced by the decrease in the viscosity at higher shear rates, which is crucial for smooth extrusion through the nozzle in extrusion-based printing [38]. In sequential shear-rate sweeps (from 0.001 to 1000 s^{-1} followed by 1000 to 0.001 s^{-1}), the viscosity of the 16.7 w/w% starch slurry was maintained. This rheological behavior supports the ability of the material to maintain its shape after extrusion. The shear-thinning behavior of the starch slurry was consistent with previous reports [18,39], which attributed shear-thinning to the breakdown of amylose and amylopectin at high shear rates [39,40].

Furthermore, we assessed the printability of the material by fabricating hexagonal constructs (Fig. 2b). The inks used in this study exhibited a viscosity below 100 mPa s (Fig. 3a), a range typically associated with poor printability and shape fidelity in 3D bioprinting [41]. This was confirmed by the fact that without the support material, the construct could not be printed (Fig. 2c), highlighting the necessity of the support. Utilizing the support material composed of 4.8 and 9.1 w/w% starch resulted in collapse of the construct (Fig. 2d,e) because of the low viscosity of the support material (Fig. 2a). A hexagonal construct faithful to the blueprint (Fig. 2b) was obtained using the support material composed of 16.7 w/w% starch (Fig. 2f), which provides adequate support. A further increase in the concentration to 28.6 w/w% hindered smooth extrusion, leading to poor printability (Fig. S5). Based on these results, 16.7 w/w% starch was selected as the most suitable support material within the tested conditions. In this study, the starch-based support material was enzymatically degraded by immersing the construct in PBS containing 0.1 w/v% α-amylase solution post-printing. This α-amylase concentration was selected because of its non-cytogenetic effects and reported cytocompatibility [42,43]. Using this method, the support material was removed within 15 min (Fig. S6).

Additionally, considering that the support material in this study not only provides structural support but also induces gelation of the bioink by supplying H_2O_2, determining a suitable H_2O_2 concentration is crucial. H_2O_2 concentrations of up to 10 mM had no significant effect on the rheological properties of the support material composed of 16.7 w/w % starch (Fig. S7). In the absence of H_2O_2, no construct was fabricated (Fig. 2g) because phenolic crosslinking did not occur, resulting in no gelation of gelatin-Ph. With the use of 1 (Fig. 2h) and 5 mM H_2O_2 (Fig. 2i), the hexagonal constructs exhibited poor geometric fidelity. By contrast, a hexagonal construct was successfully fabricated using the support material containing 10 mM H_2O_2 (Fig. 2j). These results indicate that 1 and 5 mM H_2O_2 in the support materials were insufficient to achieve adequate crosslinking. Further increasing the H_2O_2 concentration to 50 mM decreased the shape fidelity (Fig. 2k), because of nozzle clogging and uneven ink extrusion resulting from the rapid hydrogelation of the ejected ink immediately after extrusion. Previous studies have reported the dependence of hydrogelation rate on H_2O_2 concentration for HRP-mediated hydrogelation systems [28–31]. Similarly, in bioprinting, a comparably favorable concentration of 10 mM H_2O_2 was identified in previous reports using HA-Ph inks [17,30]. Based on these

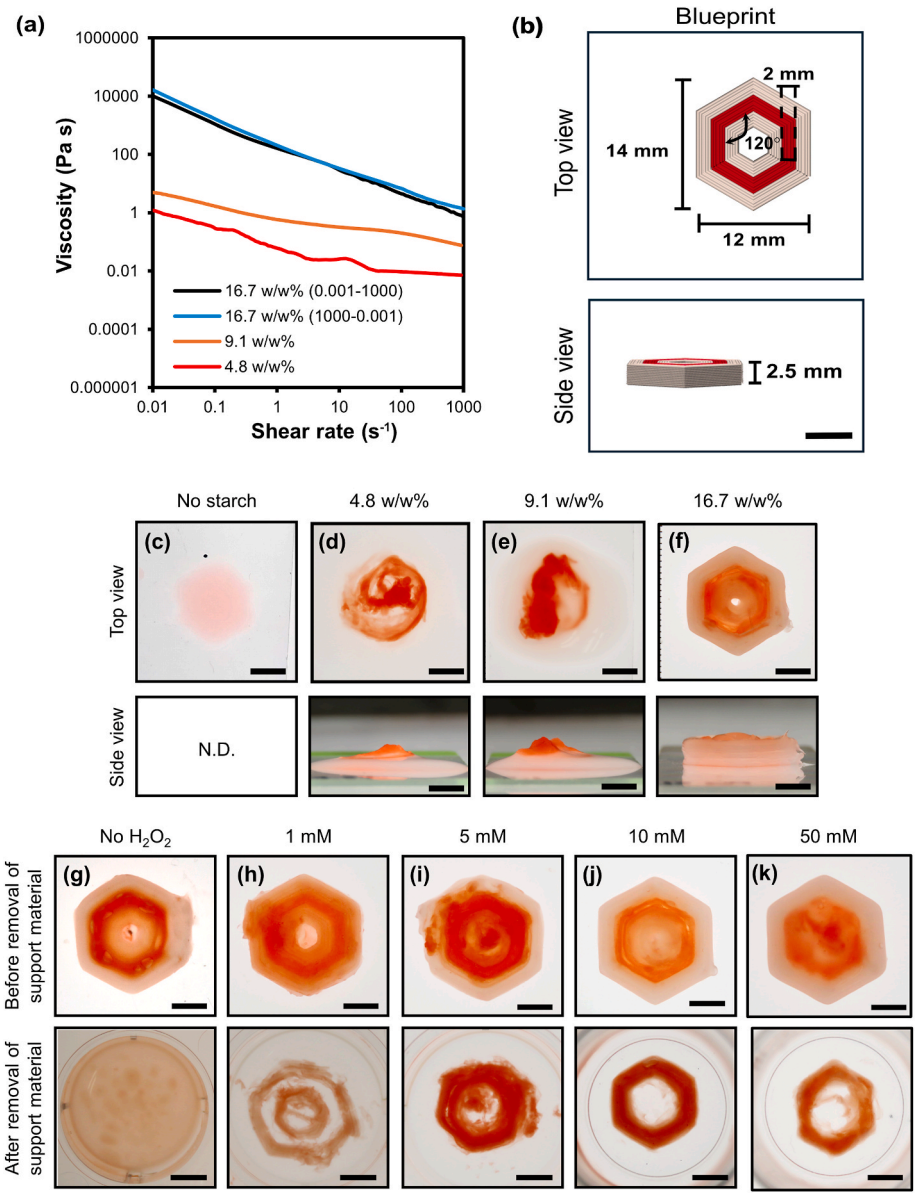

Fig. 2. (a) Viscoelastic properties of starch slurry (4.8–16.7 w/w%) at 25 °C. Measurement was conducted at a shear rate of 0.001–1000 s^{-1} for 4.8 and 9.1 w/w% starch slurries, and a cycle shear rate (decrease then increase) for 16.7 w/w% starch slurry. (b) Blueprint and photographs of hexagonal constructs printed (c) without or with support material composed of (d) 4.8, (e) 9.1, and (f) 16.7 w/w% starch + 10 mM H_2O_2. Photographs of constructs fabricated using 16.7 w/w% starch (g) without or with the addition of (h) 1, (i) 5, (j) 10, and (k) 50 mM H_2O_2. Scale bars indicate 5 mm. N.D.: no data as the ink was not gelled.

results, 10 mM H_2O_2 was determined to be the most suitable concentration within the tested range and was incorporated into the support material in the subsequent experiments.

In the fabrication of hydrogels that use H_2O_2 to induce crosslinking reactions, H_2O_2 is typically added by directly mixing it with the ink or indirectly supplying it through enzymatic or oxidation reactions [31]. However, direct mixing of the H_2O_2 solution with the ink leads to highly rapid gelation, which is difficult to control, and results in inhomogeneous crosslinking [31]. However, an indirect supply of H_2O_2 commonly leads to slow gelation, which is not suitable for the 3D printing of low-viscosity ink [44,45]. Using the method developed in this study, the diffusion of H_2O_2 from the support material delays immediate contact with the ink; however, it remains sufficiently fast to preserve the shape of the construct after printing, making it suitable for printing low-viscosity ink.

Subsequently, gelatin-Ph-based inks were evaluated to determine the most favorable conditions for fabricating 3D printed constructs using the starch-based support material. First, we evaluated the effect of ink concentration on the printability of the construct. Rheological measurements of PBS containing gelatin-Ph showed shear-thinning properties, as demonstrated by the decrease in viscosity at a higher shear rate and concentration-dependent increase in viscosity (Fig. 3a). This shear-thinning property is consistent with the results of previous studies [46, 47]. The printability was evaluated by printing a hexagonal construct (Fig. 2b), demonstrating that the polymer concentration in the ink affected the final structure (Fig. 3b). At 1.0 w/v%, the construct could not be fabricated because of its low viscosity and inability to gel. In contrast, both 2.5 and 5.0 w/v% gelatin-Ph inks enabled the fabrication of hexagonal constructs. The constructs printed with 5.0 w/v% gelatin-Ph showed geometrical dimensions (Fig. 3e–g) closer to the blueprint (Fig. 2b). Moreover, after one day of immersion in PBS, the construct fabricated using 2.5 w/v% was partially degraded (Fig. 3h). These results are attributed to the crosslinking density of phenol; gelatin-Ph concentrations lower than 5.0 w/v% did not provide

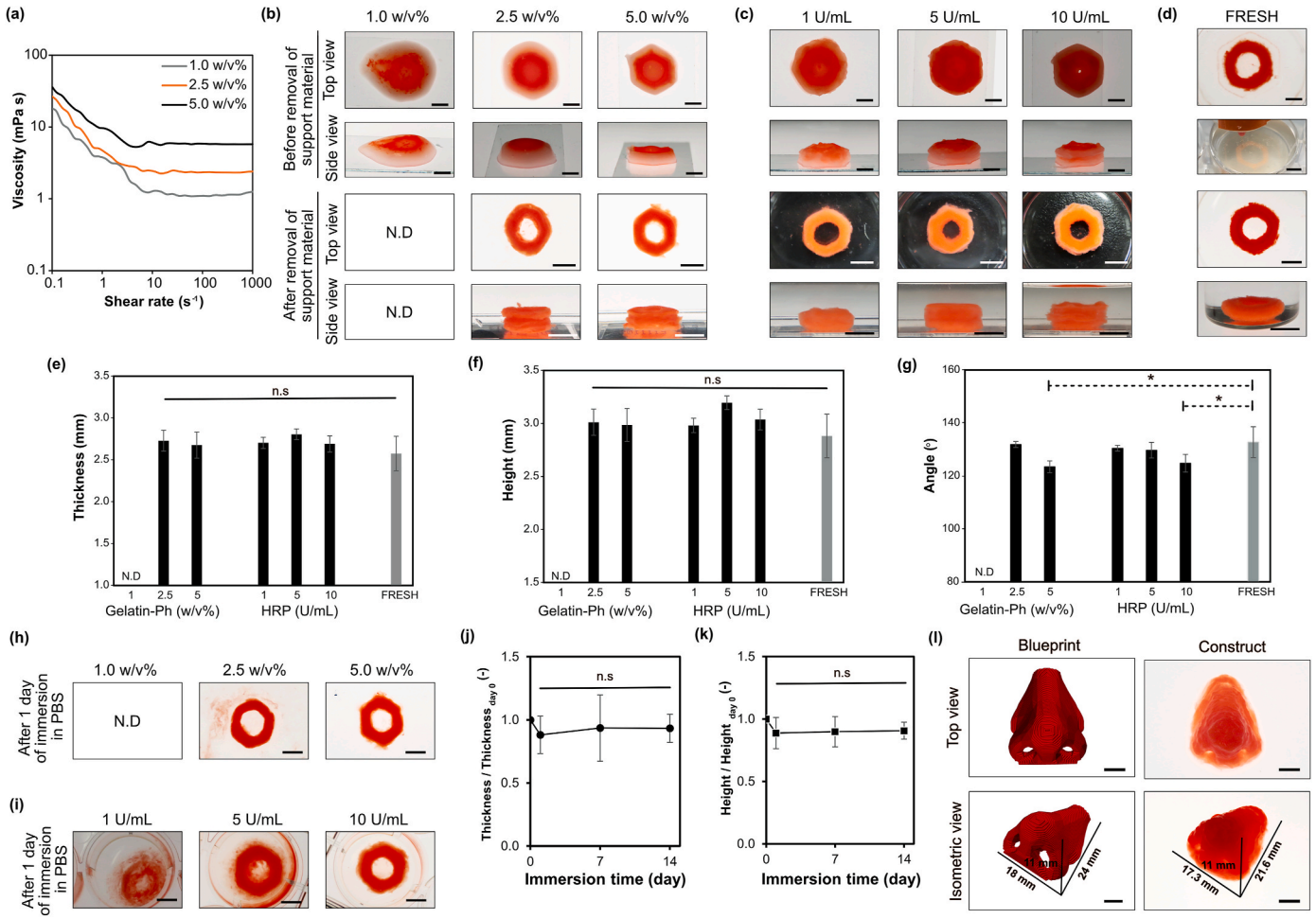

Fig. 3. (a) Viscosity–shear rate profiles of PBS containing 1.0, 2.5, and 5.0 w/v% gelatin-Ph, measured at 25 °C. (b, c) Photographs of hexagonal constructs printed with varying concentrations of (b) gelatin-Ph and (c) HRP observed before and after removal of the starch-based support material (16.7 w/w% starch + 10 mM H_2O_2). (d) Construct printed using 5 w/v% gelatin-Ph supplemented by 10 U/mL HRP using the FRESH method with a gelatin support bath containing 10 mM H_2O_2. (e–g) Construct geometry measurements, including (e) thickness, (f) height, and (g) corner angle. (h,i) Stability of constructs fabricated using varying (h) gelatin-Ph and (i) HRP concentrations after 1 day of immersion in PBS at 37 °C. Changes in (j) thickness and (k) height of constructs printed with 5.0 w/v% gelatin-Ph and 10 U/mL HRP ink following immersion in PBS at 37 °C for 14 days. (l) Blueprint and photographs of human-nose-shaped constructs printed with 5.0 w/v% gelatin-Ph and 10 U/mL HRP ink. Scale bars: 5 mm. Error bars: S.D. ($n = 3$). n.s., no significant difference ($p > 0.05$), *$p < 0.05$, Tukey HSD; N.D., no data as constructs were broken.

sufficient crosslinking to allow the construct to maintain its shape [17, 30]. Considering the fidelity of the hexagonal construct relative to the blueprint, and the post-printing stability, a gelatin-Ph concentration of 5.0 w/v% was selected for this study.

Next, we evaluated the influence of the HRP concentration in the ink. The hexagonal constructs were successfully fabricated using the inks containing 1, 5, and 10 U/mL HRP (Fig. 3c). An increase in HRP concentration improved shape fidelity (Fig. 3e–g) by providing sufficient crosslinking density [17]. Although the thickness (Fig. 3e) and height (Fig. 3f) of constructs printed with 1 U/mL were comparable to those fabricated with 10 U/mL, this was mainly due to degradation, as the 1 U/mL constructs were completely degraded one day after printing (Fig. 3i). Additionally, constructs printed with 5 U/mL HRP also exhibit partial degradation on day 1 post-immersion in PBS (Fig. 3i). These results can be attributed to insufficient crosslinking at low HRP concentrations, which results in lower stability of the hydrogel construct [17,48]. Based on these findings, 5.0 w/v% gelatin-Ph and 10 U/mL HRP were selected as the preferred ink formulations.

To validate the performance of the 3D printing method developed in this study, FRESH printing was performed using a gelatin microparticle slurry bath. Embedded 3D printing techniques, including the FRESH method, are widely used for 3D printing using low-viscosity inks [15,16, 49]. This comparison enabled evaluation of whether the developed method met or surpassed the established requirements for low-viscosity ink printing. The results showed that hexagonal constructs were successfully printed using both methods (Fig. 3b–d). Comparison in the geometry of the printed construct between our method and FRESH printing showed that despite a comparable thickness (Fig. 3e) and height (Fig. 3f) was observed, the corner angles of the construct printed with the starch support material were significantly closer ($p < 0.05$, Tukey HSD) to the blueprint (Fig. 2b) than the construct printed using the FRESH method (Fig. 3g). This is plausibly because the starch slurry provided greater shear resistance and rigidity (Fig. S8), which supported the extruded filaments more effectively and helped maintain sharper corners during printing [50–52]. Another notable difference between these two methods is the amount of support material required. The FRESH method typically requires a relatively large volume of gelatin slurry to prevent distortion during printing [16,53], whereas the starch-based method requires a much smaller amount of support material, making it easier to prepare, reduces waste, and increases the potential for large-scale production.

Next, we further evaluated the stability of the constructs printed under favorable ink and starch support material conditions. No significant changes ($p > 0.05$, one-way ANOVA) were observed in the thickness or height (Fig. 3j,k, Fig. S9) of the constructs after immersion in PBS for 14 days. Consistent with this finding, several previous studies also

reported the stability of constructs printed using phenol-conjugated polymers as inks in an HRP-mediated crosslinking system [33,54].

To further validate the robustness of the most suitable conditions identified in this study, including the inks containing 5.0 w/v% gelatin-Ph and 10 U/mL HRP, and the support material composed of 16.7 w/w% starch and 10 mM H_2O_2, a construct shaped like a human nose featuring overhangs and internal holes was successfully printed (Fig. 3l), serving as a representative example of a more geometrically complex structure. The printed dimensions of the construct closely matched the blueprints, indicating satisfactory shape fidelity and printability. The slightly shorter length and width of the construct compared to the blueprint were attributed to the shrinkage behavior of the gelatin-Ph hydrogel [17]. Although the construct was initially printed with high fidelity to the blueprint (Fig. 2b), shrinkage occurred after starch removal (Fig. S10). This result confirms that the combination of the gelatin-Ph/HRP bioink and starch/H_2O_2 support material enables the fabrication of geometrically intricate structures, with the support material effectively preventing deformation during printing and being removable without compromising the integrity of the construct. Overall, the present results demonstrate the applicability of this printing system to the fabrication of stable and complex 3D structures.

3.2. Evaluation of viability and growth of stem cells in the printed construct

Next, we applied this system to fabricate cell-laden constructs. The UE7T-13 cells were then incorporated into the bioink. Fluorescence micrographs showed that the cell-laden hexagonal constructs maintained their shape throughout 14 days of culture (Fig. 4a). Confocal microscopy with calcein-AM/PI staining showed that UE7T-13 cells remained predominantly viable from days 1–14 of culture (Fig. 4b). Quantitative analysis of the green and red fluorescence signals revealed that the printed cells exhibited a viability rate of 80.1 ± 4.3 % one-day post-printing. Additionally, the cells remained metabolically active during this period (Fig. 4c). Similar results were obtained using mouse fibroblast BALB/3T3 cells (Fig. S11). These results demonstrate that the gelatin-Ph-based bioinks and printing system induced minimal cell damage, allowing the cells to maintain their viability and metabolic activity. In addition to the well-known cytocompatibility of gelatin-Ph, the use of a relatively low concentration of H_2O_2, followed by extensive washing and quenching with catalase, also reduced possible cytotoxic effects [27]. The low flow rate during printing (1.5–3.0 μL/s), coupled with the tapered nozzle geometry, reduces the shear stress applied to the cells during printing [55], further preserving the cell viability.

Furthermore, for 3D bioprinting using support materials, it is important to ensure that the mechanism of removing the support material is cytocompatible. Conventional removal methods employing significant pH changes, temperature fluctuations, excessive washing, and sonication can compromise cell viability and alter cellular behavior [10,16,53,56,57]. To develop a cell-friendly removal method, the starch support material was degraded via a mild enzymatic reaction using α-amylase. Moreover, enzymatic reactions can be carried out under physiological conditions, making the process simple and cell-friendly [24,58]. This reaction is also selective for starch, minimizing the risk of damage to the printed construct.

Furthermore, the UE7T-13 cells exhibited an elongated morphology (Fig. 4b). The increased metabolic activity (Fig. 4c), coupled with the apparent increase in the cell number in the confocal micrographs from days 1 to 14 of culture (Fig. 4b), indicated the growth of UE7T-13 cells in the printed construct. In addition to the presence of the RGD-tripeptide, gelatin-Ph can be remodeled by cells via matrix metalloproteinases (MMP)-mediated degradation, facilitating the elongation and growth of cells in the construct [59–61]. Moreover, a stiff construct exerts a force on the enclosed cells, inhibiting cell growth and elongation, whereas a softer construct allows both processes [62,63]. Overall, these results demonstrate the applicability of this system for fabricating soft 3D constructs that support the elongation and growth of enclosed cells.

3.3. Evaluation of stemness and osteogenic differentiation of stem cells enclosed in the construct

The stemness of the UE7T-13 cells enclosed in the printed constructs was also evaluated. Maintaining stemness is essential for mesenchymal stem cells (MSCs) to self-renew, proliferate, and differentiate [64,65]. In 3D bioprinting, the printing process may influence the properties of cells, including their stemness [66,67]. However, stem cells must retain their properties when used for bioprinting. Therefore, the development of a 3D bioprinting system that preserves the stem cell properties is crucial [68].

We investigated the key stemness markers of the 3D bioprinted UE7T-13 cells through RT-qPCR analysis of the expression of CD105 and Sox2, as well as flow cytometry analysis of CD44 and CD45 after 14 days of culture (Fig. 5a). The initial stemness of the 3D bioprinted cells, measured by assessing the CD105 and Sox2 expression levels, was comparable to that of the cells cultured on a dish (Fig. S12). Stable expression of CD105 (Fig. 5b) and Sox2 genes (Fig. 5c) in the 3D bioprinted UE7T-13 cells was observed from days 1–14 of culture, whereas in the 2D-cultured UE7T-13 cells, the CD105 and Sox2 expression decreased on day 14 (Fig. S12). Additionally, the stemness of the 3D bioprinted UE7T-13 cells was further confirmed by comparable expression of the MSCs-positive marker CD44 (Fig. 5d) and negative

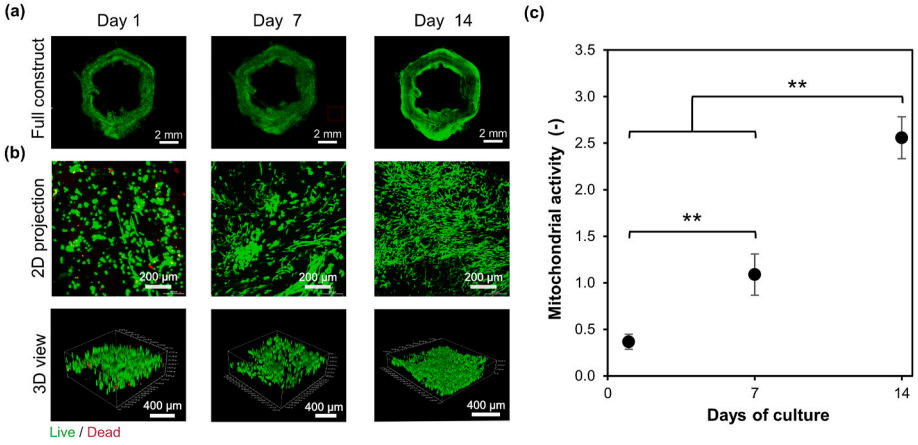

Fig. 4. (a) Fluorescence and (b) confocal micrographs of UE7T-13 cells enclosed in 3D bioprinted constructs stained with calcein-AM (green: live cells) and PI (red: dead cells). (c) Mitochondrial activity of UE7T-13 cells per construct after 1, 7, and 14 days of culture. Error bars indicate S.D. ($n = 3$). $^{**}p < 0.005$, Tukey HSD.

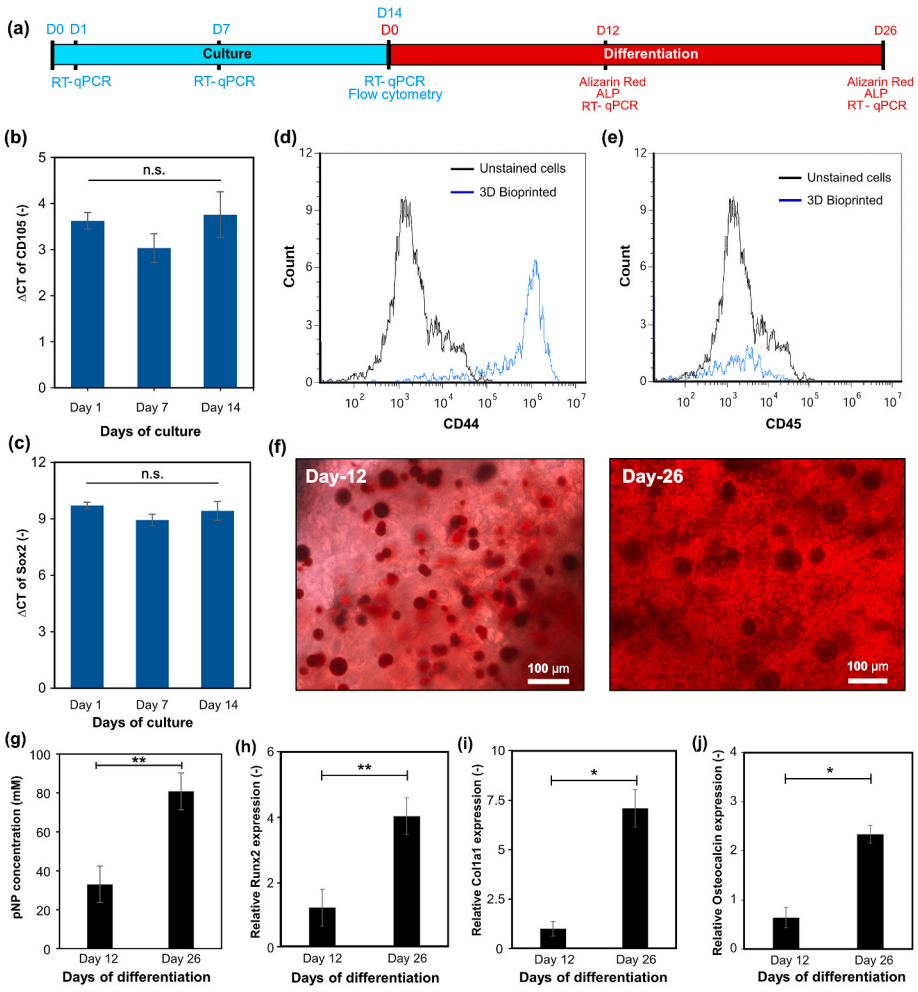

Fig. 5. (a) Experimental timeline for evaluation of stemness and osteogenic differentiation of UE7T-13 cells enclosed in the printed construct. (b–e) Evaluation of stemness based on relative expression of (b) CD105 and (c) Sox2 genes after 1, 7, and 14 days of culture and flow cytometry of (d) CD44 and (e) CD45 on day 14 of culture. (f–j) Assessment of osteogenic differentiation of the 3D bioprinted UE7T-13 cells: (f) alizarin red staining, (g) alkaline phosphatase activity, and gene expression of (h) Runx2, (i) Col1a1, and (j) osteocalcin genes, relative to those of undifferentiated cells. Differentiation was conducted after an initial 14 days of enclosure. Error bars indicate S.D. ($n = 3$). n.s: no significant difference ($p > 0.05$), *$p < 0.05$, **$p < 0.005$, Tukey HSD.

marker CD45 (Fig. 5e). These findings indicate that the 3D bioprinting process and long-term enclosure of the gelatin-Ph constructs did not affect the stemness of the cells.

Extrusion-based 3D bioprinting has been reported to generate more shear stress and alter the cellular properties [66,67,69]. This high shear stress is primarily attributable to the use of high-viscosity bioinks, which are commonly required for extrusion-based 3D printing [69]. However, in this study, a low-viscosity ink was used, thereby eliminating the high shear stress associated with the ink viscosity [67]. Additionally, the tapered nozzle and low flow rate did not significantly affect the stemness of the MSCs [7,55,69]. Furthermore, 3D cultures on hydrogels provide biophysical, biochemical, and mechanical cues that support the preservation of stemness [70–72].

Finally, to confirm that the UE7T-13 cells retained their ability to differentiate after 14 days of enclosure, we assessed their capacity for osteogenic differentiation. Osteogenic differentiation was induced by replacing the culture medium with the differentiation medium on day 14 (Fig. 5a). Differentiation was induced for 26 days, and the osteogenic differentiation was assessed using alizarin red staining and analysis of the alkaline phosphatase activity and RT-qPCR on days 12 and 26 of differentiation.

Calcium deposition, as assessed by alizarin red staining, was observed on days 12 and 26 of differentiation (Fig. 5f). On day 12, red-stained regions was observed, indicating the onset of mineralization [73–75]. By day 26, the staining intensity increased markedly, with calcium deposition distributed throughout the construct (Fig. 5f). Diffusion limitations, which cause uneven mineralization, are among the main concerns in the application of 3D hydrogels as scaffolds for bone regeneration [76,77]. However, in the present study, calcium deposition was observed in both the outer and core regions of the construct (Fig. S13), demonstrating uniform mineralization. Next, we assessed the activity of alkaline phosphatase (ALP), an osteogenic differentiation marker essential for mineralization. ALP hydrolyzes phosphate groups to generate inorganic phosphates for hydroxyapatite formation [78]. The ALP activity was evaluated by measuring the conversion of *p*-nitrophenylphosphate (*p*NPP) to yellow *p*-nitrophenolate (*p*NP) [79]. As shown in Fig. 5g, elevated *p*NP production, indicating increased ALP activity, was observed from days 12–26 of differentiation. The significant increase in the ALP activity indicated that the UE7T-13 cells successfully transitioned into the osteoblast lineage [80]. Additionally, the increased ALP activity and calcium deposition (as shown by alizarin red staining) confirmed that ECM mineralization was still actively progressing on day 26.

The differentiation of the printed UE7T-13 cells into osteoblasts was further characterized by analyzing the expression of osteoblast genes. The RT-qPCR results showed a significant increase in expression of Runx2 (Fig. 5h), Col1a1 (Fig. 5i), and osteocalcin (Fig. 5j) from days 12–26 of differentiation. The commitment of MSCs to the osteoblast

lineage is facilitated by the upregulation of Runx2 [80]. The high expression of Runx2, Osteocalcin, and Col1a1 also provides evidence supporting active engagement of the osteoblasts in ECM production and mineralization [81,82].

Overall, the increase in the alizarin red staining, ALP activity, and osteoblast gene expression from days 12–26 of differentiation (Fig. 5f–j) demonstrates the time-dependent progression of osteogenic differentiation. By day 26, the cells transitioned into mature osteoblasts capable of producing a mineralized extracellular matrix, which is a hallmark of bone tissue formation [81].

These findings demonstrate the usefulness of starch as a support material for 3D bioprinting. Future studies should address the limitations of this study. To achieve constructs with higher fidelity and resolution, the printing process, including the G-codewhich governs the nozzle movement during printing, must be further optimized. Moreover, a comparative study is needed to identify the starch type most suitable for use as a support material, as the viscosity of starch slurry depends on its origin t [83]. To further strengthen our validation of the applicability of the developed 3D bioprinting method, a more comprehensive study using various bioinks must be conducted in the future. Additionally, MSCs-specific surface markers, including positive markers of CD73 and CD90 and negative markers of CD34, CD14, CD19, and HLA-DR, must be analyzed thoroughly. Furthermore, the differentiation potential of printed MSCs into chondrogenic and adipogenic lineages needs to be investigated.

4. Conclusions

In this study, we demonstrated the utility of starch as a support material for fabricating cell-laden constructs by alternately extruding low-viscosity bioinks composed of gelatin-Ph, HRP, and UE7T-13 cells with starch-based support materials supplemented with H_2O_2. The support materials provide structural support and induce HRP-catalyzed gelation of the bioinks while allowing easy post-printing removal by immersion in α-amylase solution. This system enables the fabrication of complex and stable 3D structures. The UE7T-13 cells enclosed in the bioprinted constructs maintained their physiological functions, including viability, elongated morphology, growth, and stemness throughout the 14 days of culture. The UE7T-13 cells enclosed in the construct also differentiated into an osteogenic lineage. Overall, the present findings highlight the potential of this bioprinting method for fabricating cell-laden constructs for diverse tissue-engineering applications.

CRediT authorship contribution statement

Pekik Wiji Prasetyaningrum: Writing – review & editing, Writing – original draft, Visualization, Methodology, Investigation, Data curation, Conceptualization. **Wildan Mubarok:** Writing – review & editing, Writing – original draft, Visualization, Investigation, Formal analysis, Data curation. **Takashi Kotani:** Writing – review & editing, Software, Methodology, Investigation, Data curation. **Shinji Sakai:** Writing – review & editing, Writing – original draft, Supervision, Resources, Methodology, Funding acquisition, Conceptualization.

Declaration of competing interest

The authors declare that they have no known competing financial interests or personal relationships that could have appeared to influence the work reported in this paper.

Acknowledgements

This study was funded by the Adaptable and Seamless Technology Transfer Program through Target-Driven R&D (A-STEP) of the Japan Science and Technology Agency, Japan (grant number JPMJTR234C). P. W.P. acknowledges the support from the Ministry of Education, Culture, Sports, Science, and Technology (MEXT) scholarship of Japan. We would like to thank Editage (www.editage.jp) for the English language editing.

Appendix A. Supplementary data

Supplementary data to this article can be found online at https://doi.org/10.1016/j.bprint.2025.e00439.

Data availability

Data are available from the corresponding author upon reasonable request.

References

[1] J.J.J. Dharmaraj, R.J.H. Navasingh, G. Krolczyk, S.V. Pitcnosei, Extrusion-based bioprinting in a cost-effective bioprinter, Machines 12 (2024) 518, https://doi.org/10.3390/machines12080518.
[2] J.K. Placone, A.J. Engler, Recent advances in extrusion-based 3D printing for biomedical applications, Adv. Healthcare Mater. 7 (2018) 1701161, https://doi.org/10.1002/adhm.201701161.
[3] K.A. Deo, K.A. Singh, C.W. Peak, D.L. Alge, A.K. Gaharwar, Bioprinting 101: design, fabrication, and evaluation of cell-laden 3D bioprinted scaffolds, Tissue Eng. 26 (2020) 318–338, https://doi.org/10.1089/ten.tea.2019.0298.
[4] L. Ouyang, Pushing the rheological and mechanical boundaries of extrusion-based 3D bioprinting, Trends Biotechnol. 40 (2022) 891–902, https://doi.org/10.1016/j.tibtech.2022.01.001.
[5] A.S. Theus, L. Ning, B. Hwang, C. Gil, S. Chen, A. Wombwell, R. Mehta, V. Serpooshan, Bioprintability: physiomechanical and biological requirements of materials for 3d bioprinting processes, Polymers 12 (2020) 2262, https://doi.org/10.3390/polym12102262.
[6] M. Köpf, R. Nasehi, F. Kreimendahl, S. Jockenhoevel, H. Fischer, Bioprinting-associated shear stress and hydrostatic pressure affect the angiogenic potential of human umbilical vein endothelial cells, Int. J. Bioprint. 8 (2022) 96–107, https://doi.org/10.18063/ijb.v8i4.606.
[7] C. Zhang, K.C.M.L. Elvitigala, W. Mubarok, Y. Okano, S. Sakai, Machine learning-based prediction and optimisation framework for as-extruded cell viability in extrusion-based 3D bioprinting, Virtual Phys. Prototyp. 19 (2024) e2400330, https://doi.org/10.1080/17452759.2024.2400330.
[8] E. Mirdamadi, J.W. Tashman, D.J. Shiwarski, R.N. Palchesko, A.W. Feinberg, FRESH 3D bioprinting a full-size model of the human heart, ACS Biomater. Sci. Eng. 6 (2020) 6453–6459, https://doi.org/10.1021/acsbiomaterials.0c01133.
[9] M. Becker, M. Gurian, M. Schot, J. Leijten, Aqueous two-phase enabled low viscosity 3D (LoV3D) bioprinting of living matter, Adv. Sci. 10 (2023) 2204609, https://doi.org/10.1002/advs.202204609.
[10] R. Suntornnond, J. An, C.K. Chua, Roles of support materials in 3d bioprinting - present and future, Int. J. Bioprint. 3 (2017) 83–86, https://doi.org/10.18063/IJB.2017.01.006.
[11] M. Caiado Decarli, H.P. Ferreira, R. Sobreiro-Almeida, F.C. Teixeira, T.R. Correia, J. Babilotte, J. Olijve, C.A. Custódio, I.C. Gonçalves, C. Mota, J.F. Mano, L. Moroni, Embedding bioprinting of low viscous, photopolymerizable blood-based bioinks in a crystal self-healing transparent supporting Bath, Small Methods 9 (2025) 2400857, https://doi.org/10.1002/smtd.202400857.
[12] A. Lee, A.R. Hudson, D.J. Shiwarski, J.W. Tashman, T.J. Hinton, S. Yerneni, J. M. Bliley, P.G. Campbell, A.W. Feinberg, 3D bioprinting of collagen to rebuild components of the human heart, Science 365 (2019) 482–487, https://doi.org/10.1126/science.aav9051, 1979.
[13] P. Chaurasia, R. Singh, S.K. Mahto, FRESH-based 3D bioprinting of complex biological geometries using chitosan bioink, Biofabrication 16 (2024) 045007, https://doi.org/10.1088/1758-5090/ad5d18.
[14] S. Sakai, T. Morita, One-step FRESH bioprinting of low-viscosity silk fibroin inks, ACS Biomater. Sci. Eng. 8 (2022) 2589–2597, https://doi.org/10.1021/acsbiomaterials.2c00269.
[15] D.J. Shiwarski, A.R. Hudson, J.W. Tashman, A.W. Feinberg, Emergence of FRESH 3D printing as a platform for advanced tissue biofabrication, APL Bioeng. 5 (2021) 010904, https://doi.org/10.1063/5.0032777.
[16] L.G. Brunel, S.M. Hull, S.C. Heilshorn, Engineered assistive materials for 3D bioprinting: support baths and sacrificial inks, Biofabrication 14 (2022) 032001, https://doi.org/10.1088/1758-5090/ac6bbe.
[17] T. Kotani, W. Mubarok, T. Hananouchi, S. Sakai, Horseradish peroxidase-mediated bioprinting via bioink gelation by alternately extruded support material, ACS Biomater. Sci. Eng. 9 (2023) 5804–5812, https://doi.org/10.1021/acsbiomaterials.3c00996.
[18] L. Zheng, J. Liu, R. Liu, Y. Xing, H. Jiang, 3D printing performance of gels from wheat starch, flour and whole meal, Food Chem. 356 (2021) 129546, https://doi.org/10.1016/j.foodchem.2021.129546.
[19] L. Zhang, T. Zheng, L. Wu, Q. Han, S. Chen, Y. Kong, G. Li, L. Ma, H. Wu, Y. Zhao, Y. Yu, Y. Yang, Fabrication and characterization of 3D-printed gellan gum/starch

composite scaffold for Schwann cells growth, Nanotechnol. Rev. 10 (2021) 50–61, https://doi.org/10.1515/ntrev-2021-0004.
[20] S. Li, J. Li, J. Xu, Y. Shen, X. Shang, H. Li, J. Wang, Y. Liu, L. Qiang, Z. Qiao, J. Wang, Y. He, Y. Hu, Removal-free and multicellular suspension bath-based 3D bioprinting, Adv. Mater. 36 (2024) 2406891, https://doi.org/10.1002/adma.202406891.
[21] S. Liu, T. Wang, S. Li, X. Wang, Application status of sacrificial biomaterials in 3D bioprinting, Polymers 14 (2022) 2182, https://doi.org/10.3390/polym14112182.
[22] C. Wang, Y. Zhou, Sacrificial biomaterials in 3D fabrication of scaffolds for tissue engineering applications, J. Biomed. Mater. Res. B Appl. Biomater. 112 (2024) e35312, https://doi.org/10.1002/jbm.b.35312.
[23] A. Thomas, I. Orellano, T. Lam, B. Noichl, M.A. Geiger, A.K. Amler, A.E. Kreuder, C. Palmer, G. Duda, R. Lauster, L. Kloke, Vascular bioprinting with enzymatically degradable bioinks via multi-material projection-based stereolithography, Acta Biomater. 117 (2020) 121–132, https://doi.org/10.1016/j.actbio.2020.09.033.
[24] K. Date, T. Yamazaki, Y. Toyoda, K. Hoshi, H. Ogawa, α-Amylase expressed in human small intestinal epithelial cells is essential for cell proliferation and differentiation, J. Cell. Biochem. 121 (2020) 1238–1249, https://doi.org/10.1002/jcb.29357.
[25] S. Sakai, K. Hirose, K. Taguchi, Y. Ogushi, K. Kawakami, An injectable, in situ enzymatically gellable, gelatin derivative for drug delivery and tissue engineering, Biomaterials 30 (2009) 3371–3377, https://doi.org/10.1016/j.biomaterials.2009.03.030.
[26] O. Hasturk, K.E. Jordan, J. Choi, D.L. Kaplan, Enzymatically crosslinked silk and silk-gelatin hydrogels with tunable gelation kinetics, mechanical properties and bioactivity for cell culture and encapsulation, Biomaterials 232 (2020) 119720, https://doi.org/10.1016/j.biomaterials.2019.119720.
[27] W. Mubarok, K.C.M.L. Elvitigala, S. Sakai, Tuning myogenesis by controlling gelatin hydrogel properties through hydrogen peroxide-mediated cross-linking and degradation, Gels 8 (2022) 387, https://doi.org/10.3390/gels8060387.
[28] W. Mubarok, Y. Qu, S. Sakai, Influence of hydrogen peroxide-mediated cross-linking and degradation on cell-adhesive gelatin hydrogels, ACS Appl. Bio Mater. 4 (2021) 4184–4190, https://doi.org/10.1021/acsabm.0c01675.
[29] W. Mubarok, C. Zhang, S. Sakai, 3D bioprinting of sugar beet pectin through horseradish peroxidase-catalyzed cross-linking, ACS Appl. Bio Mater. 7 (2024) 3506–3514, https://doi.org/10.1021/acsabm.4c00418.
[30] S. Sakai, T. Kotani, R. Harada, R. Goto, T. Morita, S. Bouissil, P. Dubessay, G. Pierre, P. Michaud, R. El Boutachfaiti, M. Nakahata, M. Kojima, E. Petit, C. Delattre, Development of phenol-grafted polyglucuronic acid and its application to extrusion-based bioprinting inks, Carbohydr. Polym. 277 (2022) 118820, https://doi.org/10.1016/j.carbpol.2021.118820.
[31] S. Sakai, M. Nakahata, Horseradish peroxidase catalyzed hydrogelation for biomedical, biopharmaceutical, and biofabrication applications, Chem. Asian J. 12 (2017) 3098–3109, https://doi.org/10.1002/asia.201701364.
[32] S.D. Kim, S. Jin, S. Kim, D. Son, M. Shin, Tyramine-functionalized alginate-collagen hybrid hydrogel inks for 3D-Bioprinting, Polymers 14 (2022) 3173, https://doi.org/10.3390/polym14153173.
[33] S. Sakai, K. Mochizuki, Y. Qu, M. Mail, M. Nakahata, M. Taya, Peroxidase-catalyzed microextrusion bioprinting of cell-laden hydrogel constructs in vaporized ppm-level hydrogen peroxide, Biofabrication 10 (2018) 045007, https://doi.org/10.1088/1758-5090/aadc9e.
[34] T.L. Ramos, L.I. Sánchez-Abarca, S. Muntión, S. Preciado, N. Puig, G. López-Ruano, Á. Hernández-Hernández, A. Redondo, R. Ortega, C. Rodríguez, F. Sánchez-Guijo, C. Del Cañizo, MSC surface markers (CD44, CD73, and CD90) can identify human MSC-derived extracellular vesicles by conventional flow cytometry, Cell Commun. Signal. 14 (2016) 2, https://doi.org/10.1186/s12964-015-0124-8.
[35] P. Guo, J. Yu, L. Copeland, S. Wang, S. Wang, Mechanisms of starch gelatinization during heating of wheat flour and its effect on in vitro starch digestibility, Food Hydrocoll. 82 (2018) 370–378, https://doi.org/10.1016/j.foodhyd.2018.04.012.
[36] M. Mariotti, M. Zardi, M. Lucisano, M.A. Pagani, Influence of the heating rate on the pasting properties of various flours, Starch/Staerke 57 (2005) 564–572, https://doi.org/10.1002/star.200500425.
[37] Z. Wang, S. Ma, B. Sun, F. Wang, J. Huang, X. Wang, Q. Bao, Effects of thermal properties and behavior of wheat starch and gluten on their interaction: a review, Int. J. Biol. Macromol. 177 (2021) 474–484, https://doi.org/10.1016/j.ijbiomac.2021.02.175.
[38] A. Schwab, R. Levato, M. D'Este, S. Piluso, D. Eglin, J. Malda, Printability and shape fidelity of bioinks in 3D bioprinting, Chem. Rev. 120 (2020) 11028–11055, https://doi.org/10.1021/acs.chemrev.0c00084.
[39] A. Heydari, S.M.A. Razavi, Rheological, functional and thermal properties of the blend system of canary seed starch-wheat starch gels, J. Food Meas. Char. 14 (2020) 3345–3360, https://doi.org/10.1007/s11694-020-00581-3.
[40] P. Kilbride, M.V. Rull, A. Townsend, H. Wilson, J. Morris, Shear-thickening fluids in biologically relevant agents, Biorheology 56 (2019) 39–50, https://doi.org/10.3233/BIR-180196.
[41] M.A. Habib, B. Khoda, Rheological analysis of bio-ink for 3D bio-printing processes, J. Manuf. Process. 76 (2022) 708–718, https://doi.org/10.1016/j.jmapro.2022.02.048.
[42] V. Silano, J.M. Barat Baviera, C. Bolognesi, B.J. Brüschweiler, P.S. Cocconcelli, R. Crebelli, D.M. Gott, K. Grob, E. Lampi, A. Mortensen, G. Rivière, I.L. Steffensen, C. Tlustos, H. Van Loveren, L. Vernis, H. Zorn, K.D. Jany, B. Glandorf, A. Penninks, D. Želježic, M. Andryszkiewicz, D. Arcella, Y. Liu, A. Rossi, K.H. Engel, A. Chesson, Safety evaluation of the food enzyme alpha-amylase from non-genetically modified Aspergillus niger strain (strain DP-Azb60), EFSA J. 17 (2019) 5680, https://doi.org/10.2903/j.efsa.2019.5680.
[43] V.J. Sewalt, T.F. Reyes, Q. Bui, Safety evaluation of two α-amylase enzyme preparations derived from Bacillus licheniformis expressing an α-amylase gene from Cytophaga species, Regul. Toxicol. Pharmacol. 98 (2018) 140–150, https://doi.org/10.1016/j.yrtph.2018.07.015.
[44] E. Gantumur, S. Sakai, M. Nakahata, M. Taya, Horseradish peroxidase-catalyzed hydrogelation consuming enzyme-produced hydrogen peroxide in the presence of reducing sugars, Soft Matter 15 (2019) 2163–2169, https://doi.org/10.1039/c8sm01839a.
[45] S. Sakai, K. Komatani, M. Taya, Glucose-triggered co-enzymatic hydrogelation of aqueous polymer solutions, RSC Adv. 2 (2012) 1502–1507, https://doi.org/10.1039/c1ra01060c.
[46] S. Sakai, H. Ohi, M. Taya, Gelatin/hyaluronic acid content in hydrogels obtained through blue light-induced gelation affects hydrogel properties and adipose stem, Biomolecules 9 (2019) 342, https://doi.org/10.3390/biom9080342.
[47] H. He, D. Li, Z. Lin, L. Peng, J. Yang, M. Wu, D. Cheng, H. Pan, C. Ruan, Temperature-programmable and enzymatically solidifiable gelatin-based bioinks enable facile extrusion bioprinting, Biofabrication 12 (2020) 045003, https://doi.org/10.1088/1758-5090/ab9906.
[48] F. Lee, K.H. Bae, M. Kurisawa, Injectable hydrogel systems crosslinked by horseradish peroxidase, Biomed. Mater. (Bristol) 11 (2015) 014101, https://doi.org/10.1088/1748-6041/11/1/014101.
[49] S. Liu, T. Wang, S. Li, X. Wang, Application status of sacrificial biomaterials in 3D bioprinting, Polymers 14 (2022) 2182, https://doi.org/10.3390/polym14112182.
[50] M.E. Cooke, D.H. Rosenzweig, The rheology of direct and suspended extrusion bioprinting, APL Bioeng 5 (2021) 011502, https://doi.org/10.1063/5.0031475.
[51] Q. Li, L. Ma, Z. Gao, J. Yin, P. Liu, H. Yang, L. Shen, H. Zhou, Regulable supporting baths for embedded printing of soft biomaterials with variable stiffness, ACS Appl. Mater. Interfaces 14 (2022) 41695–41711, https://doi.org/10.1021/acsami.2c09221.
[52] Y. Zhang, F. Huang, E. Zhang, L. Zhang, Effect of the support bath on embedded 3D printing of soft elastomeric composites, Mater. Lett. 331 (2023) 133475, https://doi.org/10.1016/j.matlet.2022.133475.
[53] M.Ö. Öztürk-Öncel, B.H. Leal-Martínez, R.F. Monteiro, M.E. Gomes, R.M. A. Domingues, A dive into the bath: embedded 3D bioprinting of freeform in vitro models, Biomater. Sci. 11 (2023) 5462–5473, https://doi.org/10.1039/d3bm00626c.
[54] E. Gantumur, M. Nakahata, M. Kojima, S. Sakai, Extrusion-based bioprinting through glucose-mediated enzymatic hydrogelation, Int. J. Bioprint. 6 (2020) 43–52, https://doi.org/10.18063/ijb.v6i1.250.
[55] M. Li, X. Tian, D.J. Schreyer, X. Chen, Effect of needle geometry on flow rate and cell damage in the dispensing-based biofabrication process, Biotechnol. Prog. 27 (2011) 1777–1784, https://doi.org/10.1002/btpr.679.
[56] L. Ouyang, R. Yao, Y. Zhao, W. Sun, Effect of bioink properties on printability and cell viability for 3D bioplotting of embryonic stem cells, Biofabrication 8 (2016) 035020, https://doi.org/10.1088/1758-5090/8/3/035020.
[57] E. Hoch, G.E.M. Tovar, K. Borchers, Bioprinting of artificial blood vessels: current approaches towards a demanding goal, Eur. J. Cardio. Thorac. Surg. 46 (2014) 767–778, https://doi.org/10.1093/ejcts/ezu242.
[58] A. Sundarram, T. Pandurangappa, K. Murthy, α-Amylase production and applications: a review, J. Appl. Environ. Microbiol. 2 (2014) 166–175, https://doi.org/10.12691/jaem-2-4-10.
[59] C. Wang, X. Tong, X. Jiang, F. Yang, Effect of matrix metalloproteinase-mediated matrix degradation on glioblastoma cell behavior in 3D PEG-based hydrogels, J. Biomed. Mater. Res. 105 (2017) 770–778, https://doi.org/10.1002/jbm.a.35947.
[60] B. Trappmann, B.M. Baker, W.J. Polacheck, C.K. Choi, J.A. Burdick, C.S. Chen, Matrix degradability controls multicellularity of 3D cell migration, Nat. Commun. 8 (2017) 371, https://doi.org/10.1038/s41467-017-00418-6.
[61] A.E. Gilchrist, S. Lee, Y. Hu, B.A.C. Harley, Soluble signals and remodeling in a synthetic gelatin-based hematopoietic stem cell niche, Adv. Healthcare Mater. 8 (2019) 1900751, https://doi.org/10.1002/adhm.201900751.
[62] S. Nam, O. Chaudhuri, Mitotic cells generate protrusive extracellular forces to divide in three-dimensional microenvironments, Nat. Phys. 14 (2018) 621–628, https://doi.org/10.1038/s41567-018-0092-1.
[63] K.M. Wisdom, K. Adebowale, J. Chang, J.Y. Lee, S. Nam, R. Desai, N.S. Rossen, M. Rafat, R.B. West, L. Hodgson, O. Chaudhuri, Matrix mechanical plasticity regulates cancer cell migration through confining microenvironments, Nat. Commun. 9 (2018) 4144, https://doi.org/10.1038/s41467-018-06641-z.
[64] C. Blanpain, W.E. Lowry, A. Geoghegan, L. Polak, E. Fuchs, Self-renewal, multipotency, and the existence of two cell populations within an epithelial stem cell niche, Cell 118 (2004) 635–648, https://doi.org/10.1016/j.cell.2004.08.012.
[65] M. Dominici, K. Le Blanc, I. Mueller, I. Slaper-Cortenbach, F.C. Marini, D.S. Krause, R.J. Deans, A. Keating, D.J. Prockop, E.M. Horwitz, Minimal criteria for defining multipotent mesenchymal stromal cells. The international society for cellular therapy position statement, Cytotherapy 8 (2006) 315–317, https://doi.org/10.1080/14653240600855905.
[66] S.A. Irvine, S.S. Venkatraman, Bioprinting and differentiation of stem cells, Molecules 21 (2016) 1188, https://doi.org/10.3390/molecules21091188.
[67] J. Snyder, A. Rin Son, Q. Hamid, C. Wang, Y. Lui, W. Sun, Mesenchymal stem cell printing and process regulated cell properties, Biofabrication 7 (2015) 044106, https://doi.org/10.1088/1758-5090/7/4/044106.
[68] H.Q. Xu, J.C. Liu, Z.Y. Zhang, C.X. Xu, A review on cell damage, viability, and functionality during 3D bioprinting, Mil. Med. Res. 9 (2022) 70, https://doi.org/10.1186/s40779-022-00429-5.
[69] A. Blaeser, D.F. Duarte Campos, U. Puster, W. Richtering, M.M. Stevens, H. Fischer, Controlling shear stress in 3D bioprinting is a key factor to balance printing

resolution and stem cell integrity, Adv. Healthcare Mater. 5 (2016) 326–333, https://doi.org/10.1002/adhm.201500677.
[70] A. Pangjantuk, P. Kaokaen, P. Kunhorm, N. Chaicharoenaudomrung, P. Noisa, 3D culture of alginate-hyaluronic acid hydrogel supports the stemness of human mesenchymal stem cells, Sci. Rep. 14 (2024) 4436, https://doi.org/10.1038/s41598-024-54912-1.
[71] R.Z. Tang, X.Q. Liu, Biophysical cues of in vitro biomaterials-based artificial extracellular matrix guide cancer cell plasticity, Mater. Today Bio 19 (2023) 100607, https://doi.org/10.1016/j.mtbio.2023.100607.
[72] J. Li, Y. Liu, Y. Zhang, B. Yao, Enhejirigala, Z. Li, W. Song, Y. Wang, X. Duan, X. Yuan, X. Fu, S. Huang, Biophysical and biochemical cues of biomaterials guide mesenchymal stem cell behaviors, Front. Cell Dev. Biol. 9 (2021) 640388, https://doi.org/10.3389/fcell.2021.640388.
[73] A. Joshi, T. Kaur, N. Singh, 3D bioprinted alginate-silk-based smart cell-instructive scaffolds for dual differentiation of human mesenchymal stem cells, ACS Appl. Bio Mater. 5 (2022) 2870–2879, https://doi.org/10.1021/acsabm.2c00251.
[74] N. Raveendran, S. Ivanovski, C. Vaquette, The effect of culture conditions on the bone regeneration potential of osteoblast-laden 3D bioprinted constructs, Acta Biomater. 156 (2023) 190–201, https://doi.org/10.1016/j.actbio.2022.09.042.
[75] M. Koblenzer, M. Weiler, A. Fragoulis, S. Rütten, T. Pufe, H. Jahr, Physiological mineralization during In vitro osteogenesis in a biomimetic spheroid culture model, Cells 11 (2022) 2702, https://doi.org/10.3390/cells11172702.
[76] D.S.A. Al Maruf, Y.A. Ghosh, H. Xin, K. Cheng, P. Mukherjee, J.M. Crook, G. G. Wallace, T.J. Klein, J.R. Clark, Hydrogel: a potential material for bone tissue engineering repairing the segmental mandibular defect, Polymers 14 (2022) 4186, https://doi.org/10.3390/polym14194186.
[77] Q. Ding, S. Zhang, X. Liu, Y. Zhao, J. Yang, G. Chai, N. Wang, S. Ma, W. Liu, C. Ding, Hydrogel tissue bioengineered scaffolds in bone repair: a review, Molecules 28 (2023) 7039, https://doi.org/10.3390/molecules28207039.
[78] S. Vimalraj, Alkaline phosphatase: structure, expression and its function in bone mineralization, Gene 754 (2020) 144855, https://doi.org/10.1016/j.gene.2020.144855.
[79] M. Jain, R.G. Vaze, S.C. Ugrani, K.P. Sharma, Mechanoresponsive and recyclable biocatalytic sponges from enzyme-polymer surfactant conjugates and nanoparticles, RSC Adv. 8 (2018) 39029–39038, https://doi.org/10.1039/c8ra08221a.
[80] S. Zhu, W. Chen, A. Masson, Y.P. Li, Cell signaling and transcriptional regulation of osteoblast lineage commitment, differentiation, bone formation, and homeostasis, Cell Discov. 10 (2024) 71, https://doi.org/10.1038/s41421-024-00689-6.
[81] T.M. Liu, E.H. Lee, Transcriptional regulatory cascades in Runx2-dependent bone development, Tissue Eng., Part B 19 (2013) 254–263, https://doi.org/10.1089/ten.teb.2012.0527.
[82] D.S. Amarasekara, S. Kim, J. Rho, Regulation of osteoblast differentiation by cytokine networks, Int. J. Mol. Sci. 22 (2021) 2851, https://doi.org/10.3390/ijms22062851.
[83] L. Zheng, Y. Yu, Z. Tong, Q. Zou, S. Han, H. Jiang, The characteristics of starch gels molded by 3D printing, J. Food Process. Preserv. 43 (2019) e13993, https://doi.org/10.1111/jfpp.13993.